Materials & Design 217 (2022) 110648

Contents lists available at ScienceDirect

Materials & Design

journal homepage: www.elsevier.com/locate/matdes

Production of cellular polymers without solid outer skins by gas dissolution foaming: A long-sought step towards new applications

D. Cuadra-Rodríguez [a,*], S. Barroso-Solares [a,b], M.A. Rodríguez-Pérez [a,b], J. Pinto [a,b]

[a] Cellular Materials Laboratory (CellMat), Condensed Matter Physics Department, University of Valladolid, Paseo Belén 7, Valladolid, 47011, Spain
[b] BioEcoUVA Research Institute on Bioeconomy, University of Valladolid, Valladolid 47011, Spain

HIGHLIGHTS

- Innovative design for producing skinless polymer foams by gas dissolution foaming.
- The gas diffusion barrier maintains high gas concentration in the polymer edges.
- Achievement of skinless polymer foams by using the gas diffusion barrier approach.
- Thin films with homogenous structures were completely foamed without solid skins.
- Porous in the outer layers expose the inner cellular structure to external medium.

GRAPHICAL ABSTRACT

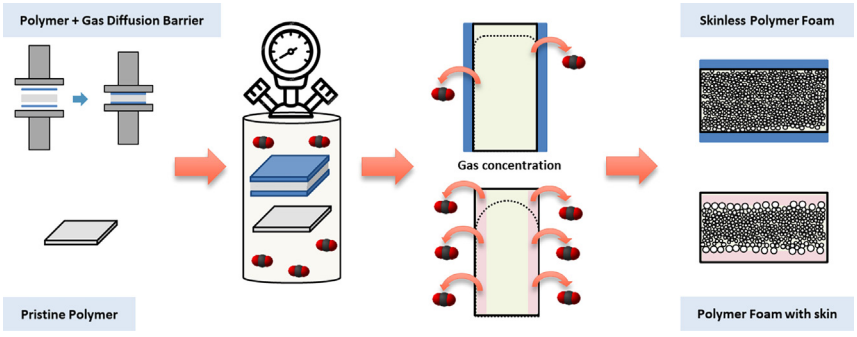

ARTICLE INFO

Article history:
Received 18 December 2021
Revised 7 April 2022
Accepted 7 April 2022
Available online 11 April 2022

Keywords:
Gas diffusion barrier
poly-vinyl alcohol (PVOH)
Gas dissolution foaming
Cellular polymers

ABSTRACT

An innovative approach to reduce and eliminate the non-foamed solid skins of the cellular polymers fabricated by gas dissolution foaming is presented in this work. The incorporation of a flexible gas diffusion barrier on the polymer surfaces during the saturation and foaming processes provided significant reduction or even hindered the appearance of the non-foamed solid skins while enabling appropriate expansions in several polymers (PMMA, PS, PC, and PCL). Besides, this approach has allowed to achieve significant expansions by foaming polymer samples with thicknesses in the order of magnitude of the non-foamed solid skins, i.e., thin films (<100 μm). This paper discusses how the gas diffusion barrier allows reducing the solid skins, the mechanisms involved in the gas diffusion process, and the possibility of interconnecting the inner cellular structure with the external medium.

1. Introduction

In the last decades, gas dissolution foaming has become one of the most used methods to fabricate cellular polymers [1,2]. This foaming process is composed of three steps: saturation (i.e., gas is dissolved into the polymer until the saturation limit), desorption (i.e., the external gas pressure is suddenly dropped), and foaming (i.e., polymer expansion, formation, and stabilization of the cellular structure). More details about this process can be found elsewhere [1,3,4]. A broad range of polymers such as poly-styrene [5], poly-carbonate [6], poly-sulfone [7], thermo-plastic polyurethane [8], and poly-methyl methacrylate [9], among others, have been successfully employed to produce micro and nanocelullar foams by gas dissolution foaming. Among other advantages, gas dissolution foaming allows achieving a fine-controlled cell size and obtaining homogeneous cellular structures by modifying the saturation and

* Corresponding author.
E-mail addresses: dcuadra@fmc.uva.es (D. Cuadra-Rodríguez), jpinto@fmc.uva.es (J. Pinto).

https://doi.org/10.1016/j.matdes.2022.110648
0264-1275/

foaming parameters [10,11]. Moreover, nanocellular polymers, which show better mechanical properties and lower thermal conductivity than microcellular ones [12–14], can be obtained using a harmless blowing agent such as carbon dioxide or nitrogen in a physical dissolution process [15] without requiring the use of toxic solvents or being limited to samples with thicknesses of a few microns [16].

In despite of the benefits and the versatility of the gas dissolution foaming compared to other methods, a significant drawback which is intrinsically involved in the fabrication process should be mentioned. The obtained samples typically show three different regions after the foaming process: a homogeneous foamed core which in bulk samples usually represents the largest volume of the sample, a non-foamed skin in the borders of the sample, and the transition between both previous regions that is characterized by a cell size gradient [17].

The presence of the non-foamed skins in the edges of the obtained foams clearly implies a limitation for using these materials in several applications such as filtration, catalysis, sensoring, adhesion, or acoustic insulation [11,18–23]. For instance, the interconnection of the cellular structure with the external medium would allow using them as filters or membranes for waste-water treatment or oil recovery [24,25]. In particular, Pinto et al. [18] produced open-cell nanocellular polymers with convenient features to act as filters, but presenting a non-foamed solid skin in the edges that avoids the interaction between the cellular structure and the external medium hindering their application as filters or membranes. On the other hand, polymer foams without non-foamed skins would also enhance their porosity and their surface area, which are interesting characteristics in catalytic processes [20]. Besides, the advantages of a completely foamed cellular polymer could result in benefit for other applications where their potential has been probed, for instance in acoustic insulation [11,22,23,26,27].

In order to take advantage of these materials for the mentioned potential applications, some works attempted to remove the solid skin after the foaming process. For instance, Martin-de Leon et al. [28] removed the non-foamed surfaces and the region with cell size gradient by polishing in order to isolate the core of transparent nanocellular foams and determine their remarkable properties. However, the polishing process destroys or damages several layers of the cellular structure leading to a new densified skin, avoiding the exposure and the interconnection of the cellular structure with the external medium [29]. Hence, other works [23,26,30–32] which applied drilling or milling processes on the non-foamed surfaces to interconnect the cellular structure with the external medium also produced irreversible damages in the sample, and thus in the cellular structure. In particular, the application of mechanical attacks is strongly discouraged to remove the solid skin in thin films. As an alternative, Yokoyama et al. [33] achieved nanocellular thin films without solid skins by removing layers of several nanometers by Reactive Ion Etching. However, this technique employs organic solvents and offers poor results in the aim of removing tens of micron, which is the typical thickness of the solid skins in polymer foams obtained by gas dissolution foaming. On the other hand, Jose et al. [34] creates pores on the solid skins by laser ablation after solid state foaming. Nevertheless, the porosity is not well-controlled and technique is just valid for small surfaces. Accordingly, instead of removing the non-foamed skin after the foam production, one of the main objectives in the cellular polymers field is the challenge of avoiding the appearance of the non-foamed skin during the gas dissolution foaming.

It is well-known that the non-foamed skin is produced due to the quick gas loss from the outer layers of the samples once the saturation pressure is released, being the gas diffusion from the outer layers to the environment faster than the cell nucleation and growing mechanisms [35,36]. Once the gas concentration in these outer layers falls below a certain threshold, no cells can be created (see Supporting Information, Section S.1) [17]. This limitation of the gas dissolution foaming technique is particularly restricting the foaming of thin films, or micrometric and nanometric systems. These systems show comparable or even lower thicknesses than the solid skins usually formed during the foaming of bulk samples. Thus, in this kind of samples the gas diffuses out not only from the external layers, but from the entire sample, hindering the formation of cells.

Some strategies, designed to overcome this limitation, can be highlighted. Siripurapu et al. [37] introduced thin films into a metallic mould which acts as gas barrier limiting the gas diffusion through the surfaces with the highest area. In this way, the gas concentration across the sample at the foaming time, which is directly related with the nucleation density [1], increases. Using this approach, they achieved more homogenous cellular structures and larger foamed region in poly-methyl methacrylate (PMMA) thin films. Nevertheless, the saturation time is also significantly risen due to the gas diffusion constraints from the borders of the sample in contact with the mould (i.e., the gas can only diffuse into the sample from the non-covered edges), being unworkable in pieces with larger dimensions. Besides, the expansion of the constrained samples could be restricted by the rigid mould, severely limiting the density reduction (i.e., low-densities cannot be achieved) [19]. On the other hand, Morisaki et al. [38] employed ethanol as a co-solvent in a mixture with the blowing agent, obtaining a solid skin reduction, even with porosity on the surface, with the increment of ethanol concentration. However, inhomogeneous cellular structures with large defects were obtained by incorporating a co-solvent that introduces severe additional difficulties in the gas dissolution foaming.

In another attempt to reduce the non-foamed skin in cellular polymers, Ge et al. [39] produced porous polymeric membranes based on thermoplastic polyurethane (TPU) for their use as filters. They achieved ultrathin films with 20 μm of thickness which show a monolayer of pores interconnecting both top and bottom surfaces, creating cells with a diameter close to the film thickness. The approach is based on the heterogeneous nucleation induced by the contact of polyamide layers with the TPU surface. However, this approach cannot be extended to thicker samples, as it is based on the formation of cells on the external surfaces with diameters close to the film thickness [40,41]. Then, thicker samples may not form the cellular structure in the core due to the insufficient gas concentration by the quick diffusion (i.e., the polyamide layer does not act as a gas diffusion barrier). However, an approach involving a gas diffusion barrier, capable of limiting the diffusivity during the foaming process, allowed producing hollow micrometric and nanometric polymeric systems with porous surfaces by coating them with poly-vinyl alcohol (PVOH) prior to the gas dissolution foaming process [35,42].

Although several methods which concern multiple stages based on the gas dissolution foaming have been developed [35,37,42–44], none of these previous approaches has proved to be a general and versatile approach to hinder the formation of the non-foamed skin during the gas dissolution foaming process, being limited in terms of geometry or expansion, or introducing complex additional steps without providing remarkable results.

Attending to the concern (i.e., the gas concentration decrease in the borders that promotes the non-foamed solid skins), the challenge of fabricating skinless polymer foams goes through designing a method which involves a gas diffusion barrier in order to maintain high gas concentration in the borders for obtaining whole foamed polymers. This work presents the design of an innovative approach that enhances the classic gas dissolution foaming process. The incorporation of a gas diffusion barrier, such as PVOH,

has allowed for first time to reduce and to eliminate the non-foamed solid skins in polymer foams without compromising geometries or expansions. In particular, a thermoplastic PVOH was used as a flexible gas diffusion barrier with the aim of facilitating their application and allowing an appropriate expansion of the polymer during the foaming stage. Besides, thin films, which cannot foam by the conventional procedure due to their thickness, have been completely foamed without solid skins by employing the PVOH technique. As a highlight, this approach proved to be quite versatile, being effective in several polymers commonly used, such as poly-methyl methacrylate (PMMA), poly-carbonate (PC), poly-styrene (PS), or poly-caprolactone (PCL).

2. Experimental section

2.1. Materials

Four different materials were selected to validate the aim of the work. PMMA ALTUGLAS V825T, PC, PS Edistir N3840, and PCL were kindly supplied by ARKEMA (Colombes, France), by SABIC (Geleen, Netherlands), by Versalis (Barcelona, Spain), and by Sigma Aldrich Química (Tres Cantos, Madrid, Spain), respectively. Poly-vynil alcohol (PVOH) MOWIFLEX C17 was purchased from Kuraray Europe (Hattersheim am Main, Deutschland). A medical grade of CO_2 (99.9% purity) was employed as a blowing agent for foaming experiments.

2.2. Fabrication of solids

All polymers were received in the form of pellets and those selected to be foamed were thermoformed in sheets (thickness around 500 μm in PMMA, PC, and PS samples, and around 1000 μm in PCL samples) by using a hot plate press. Then, the sheets were cut in samples of 1x2.5 cm^2 and used as solid precursors in the foaming experiments. In addition, PMMA pellets were used to prepare films by solvent casting method, using chloroform as a solvent (10 wt%).

2.3. PVOH incorporation

The incorporation of the PVOH barrier by diverse approaches was optimized using PMMA films (thickness < 100 μm) and bulk (thickness around 500 μm) samples, while the versatility of the PVOH barrier was also studied with bulk samples of other polymers.

Three different methods were employed to incorporate the PVOH gas barrier to the polymer samples (Fig. 1), aiming to achieve an optimal adherence between both materials along the foaming process. It should be noticed that the PVOH would be an effective gas diffusion barrier only if kept in close contact with the polymer sample. In addition, the polymer-PVOH adhesion was studied with PMMA by using a pressure vessel equipped with an optical windows [45], which allows visualizing the sample during the pressure test and just after the depressurization (more details in the Supporting Information, Section S2).

The first two techniques to incorporate the PVOH on the polymer are based on the solvent casting method (Fig. 1a and Fig. 1b). In the first approach (Fig. 1a), PVOH was dissolved in water at 5 wt%. Then, a certain volume of the PVOH/water solution, depending on the desired thickness of the gas barrier, was dropped in a petri dish. Solvent was evaporated at room temperature and ambient pressure for at least 24 h until obtaining a solid film at the bottom of the petri dish. After, the film was introduced at vacuum for ensuring the total removing of the solvent for additional 24 h. Then, the technique was repeated with PMMA/chloroform solution (10 wt%) and PVOH/water solution again, creating three overlapped films in a sandwich-like form (PVOH/PMMA/PVOH). On the second approach, a drop of PVOH/water solution (25 wt%) was rested on the surface of the polymer sheet (PMMA, PC, PS or PCL), and left to evaporate at ambient conditions until achieving a thin film of PVOH adhered to the surface (Fig. 1b). The PVOH thickness was controlled by the amount of PVOH solution dropped into the sample. The procedure was repeated on the other side of the polymer sheet.

The film thicknesses were controlled calculating the needed mass to form a cylinder into the petri dish, whose volume was calculated from the petri dish diameter and the film thickness. Then, taking into account the density of the film, the resulting mass of the polymer was dissolved according to concentrations above mentioned.

In the last approach, the PMMA samples and PVOH layers were joined by a thermoforming procedure (Fig. 1c). PVOH films were previously fabricated with the desired thickness (<100 μm) by the solvent casting method, and then they were compressed together with the PMMA sheet or film in a sandwich-like form (PVOH/PMMA/PVOH), using a three-stage thermoforming process: 120 °C without pressure for 3 min, then 120 °C and 0.98 MPa during 1 min, and finally 0.98 MPa at room temperature.

2.4. Gas dissolution foaming

2.4.1. Foaming aspects

Sheet and films samples with and without PVOH coating were employed as precursors in the conventional gas dissolution foam-

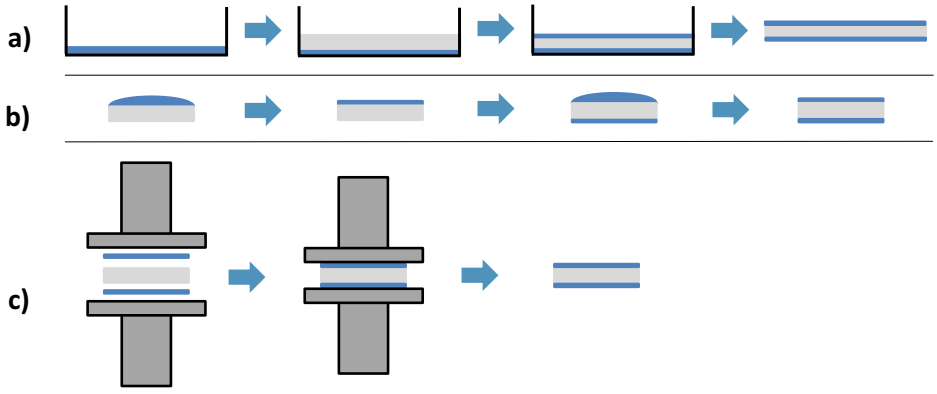

Fig. 1. PVOH incorporation methods: **a)** and **b)** solvent casting, and **c)** thermoforming. PVOH appears in blue, and the polymer to foam appears in light grey. (For interpretation of the references to colour in this figure legend, the reader is referred to the web version of this article.)

ing process [1,3,4] (e.g., saturation, desorption, and foaming steps; details about the process can be found elsewhere [1]). A high-pressure vessel (model PARR 4760) provided by Parr Instrument Company (Moline, IL, USA) was employed in the foaming procedures, following the parameters showed in Table 1. Saturation and foaming parameters were selected taking into account the properties of each polymer and previous works [46–48]. The saturation time, which depends on the sample thickness and the presence of the gas diffusion barrier among other parameters, was studied by visualizing the sample during the pressure test by following the methodology used elsewhere [45]. It was varied from 24 to 72 h to ensure the whole saturation of the polymers. More details about the influence of the gas diffusion barrier on the gas diffusivity and the setting of saturation time can be found in the Supporting Information (Section S1 and Section S2, respectively).

During the foaming stage, it is important to preserve the adhesion between both polymers for reaching a proper efficiency of the gas diffusion barrier. Thus, an oil hot bath was employed in the foaming step (instead of common water bath) to prevent the PVOH dissolution.

After the foaming process, the gas diffusion barrier was removed by introducing the samples in water (room temperature) while stirring continuously for 1 h. The removal of the gas diffusion barrier was carried out before any further characterization of the obtained foams.

This work is focused on the reduction and elimination of the non-foamed solid skins giving less importance to the relationship between the cellular structure and the foaming parameters. For that purpose see the following literature [2,9,46–50].

2.5. Characterization techniques

2.5.1. Density

Density of solid samples was measured with a gas pycnometer (Mod. AccuPyc II 1340, Micromeritics, Norcross, GA, USA), and the density of the foams was measured using the water-displacement method based on Archimedes' principle. A density determination kit for an AT261 Mettler-Toledo (Columbus, OH, USA) balance was used for this purpose. Relative density (ρ_r) was calculated from the relationship between the foam density (ρ_f) and the solid density (ρ_s) as indicates Equation (1).

$$\rho_r = \frac{\rho_f}{\rho_s} \tag{1}$$

2.5.2. Non-foamed skin measurements

The structure of the foamed samples was analyzed by Scanning Electron Microscopy (SEM) (HITACHI FlexSEM 1000). First, samples were cooled in liquid nitrogen and then fractured. Surfaces to visualize (cross-section and external surfaces achieved in samples with or without PVOH barrier) were coated with gold using a sputter coater (model SDC 005, Balzers Union, Balzers, Liechtenstein). Measurements of non-foamed skin were directly performed from SEM micrographs of the cross-section employing ImageJ/FIJI [51]. Several measures from the external edge of the sample to the homogenous cellular structure were carried out, neglecting lonely precedent pores as in the scheme shown in Fig. 2. The average thickness of both top (t_1) and bottom (t_2) non-foamed skins, and the total thickness of the foamed samples (t_t) were used to calculate the percentage of non-foamed region (NFR) (Equation (2)).

$$NFR = \frac{t_1 + t_2}{t_t} \tag{2}$$

2.5.3. Cellular structure

Cell density and cell size were analyzed from SEM micrographs in the cross-section of the homogenous core by employing a specific software based on ImageJ/FIJI [52]. First, cell density (N_v) in two dimensions was calculated taking into account the number of cells into a defined area (i.e., number of cells per square centimeter). In order to better comparison to the literature, three-dimensional values of N_v (i.e. cells/cm^3) are also provided following Kumar's theoretical approximation [53]. On the other hand, cell size (Φ) was calculated as the average value of the cell diameter measurements for at least 50 cells. Finally, porosity was estimated from Equation (3), taking advantage of the equivalence between three-dimensional and bi-dimensional values due to stereological considerations [54,55].

$$Porosity = N_v \cdot A \tag{3}$$

Where N_v is the cell density (2D) and A is the average area of the cells (assuming circular cells) calculated from the average cell size (Φ).

3. Results

3.1. Proof of concept

First, a proof of concept of the low CO_2 diffusivity presented by the PVOH was carried out incorporating the gas diffusion barrier just in one surface of a PMMA film by using the solvent casting technique (Fig. 1c), leaving the other without coating (Fig. 3).

SEM micrograph of the obtained foam shows a PMMA sample partially foamed with 220 μm of thickness (Fig. 3). The top and bottom regions of the sample present significant differences as a consequence of the use of the gas diffusion barrier, which was applied on the bottom external surface. Bottom-half of the sample is entirely occupied by a heterogeneous cellular structure. On the other hand, the top-half of the sample clearly presents a non-

Table 1
Parameters used in gas dissolution foaming for each polymer basis.

Polymer	Pressure (MPa)	Saturation temperature (°C)	Post-foaming temperature (°C)
PMMA	30	25	60
PC	30	25	100
PS	8	60	80
PCL	30	40	60

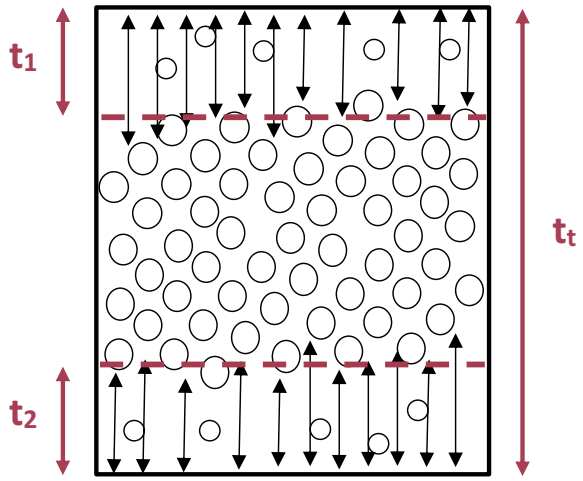

Fig. 2. Scheme of the measurement procedure of the non-foamed solid skin. Arrows indicate the distance of several measures from the edges to the homogenous cellular structure.

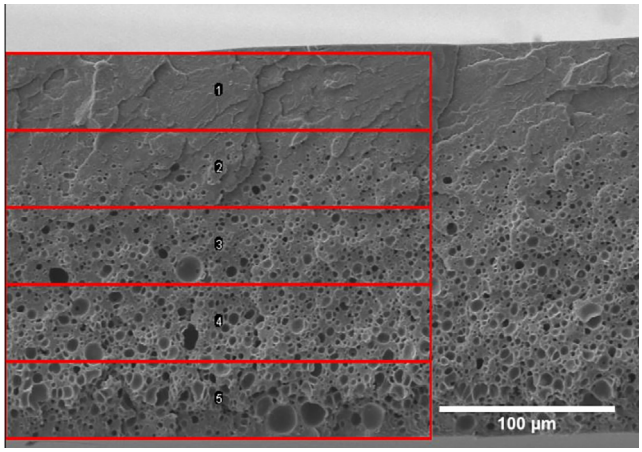

Fig. 3. SEM micrograph of PMMA film after foaming (p_{sat} = 30 MPa, T_{sat} = 25 °C, T_f = 60 °C) with PVOH technique. The gas barrier is just incorporated on the bottom surface. Squares in red represent the five analyzed regions (1: top, 2: top-middle, 3: middle, 4: bottom-middle, and 5: bottom). (For interpretation of the references to colour in this figure legend, the reader is referred to the web version of this article.)

foamed skin which represents almost 25% of the sample with a solid thickness of around 50 µm. Therefore, the PVOH barrier has allowed remaining appropriate amount of gas to foam on the bottom half of the sample, while gas located in the top half leaked through the top surface without PVOH. It must be noted that no solid skin appears on the bottom of the sample, highlighting the great effectiveness of PVOH as a gas diffusion barrier.

Besides, cellular structure shows a cell size gradient along the sample thickness, which is also promoted by the diffusion phenomenon. The number of cells per unit volume and their expansion are closely linked to the gas concentration into the polymer [1]. Thus, the gradient in gas concentration, induced by the gas diffusion out of the sample through the surfaces without PVOH, leaves a broad cell size and cell density distributions along the thickness of the sample. This effect was analyzed in the SEM micrograph by measuring both parameters in five regions along the sample thickness (Fig. 3), and the results are presented in Table 2. The largest expansions and porosities were achieved in regions 4 (bottom-middle) and 5 (bottom), while the region 1 (top) only presents a few pores. Results reveal that the gas diffusion barrier has drastically reduced the gas diffusion through the bottom surface, allowing the foaming in the bottom-half of the film. On the other hand, porosity decreases from the bottom to the top which implies that even region 3 (middle) was also affected by the gas leak through the top surface (i.e., the gas concentration at the foaming stage was lower at the center of the sample than on the bottom region near the surface covered by PVOH).

3.2. Reduction and elimination of non-foamed skins

The incorporation of PVOH on one surface of the desired polymer to foam resulted to be an excellent approach to retain higher gas concentration inside the polymer and thus both reducing the solid skin, promoting the density reduction, and achieving the foaming in thin polymer films. Therefore, an efficient incorporation of the gas barrier on both surfaces with the highest area could lead to completely foamed cellular polymers. Thus, the proposed methods to add the PVOH layer to the polymer samples (e.g., solvent casting and thermoforming) were tested in PMMA bulk samples. Solid skin measurements from SEM micrographs of PMMA bulk samples with different PVOH coating methods are showed in Table 3. Results shown in each case are the average of several samples prepared at those conditions.

It was found that the non-foamed skin thickness was reduced regardless of the PVOH incorporation method from around 80 µm to almost 10 µm in the best case (achieved by thermoforming). In this way, the percentage of non-foamed region (NFR) in PMMA without PVOH was about 20%, while the incorporation of PVOH allowed decreasing the NFR down to 2%. SEM micrographs of corresponding samples of Table 3 are available in the Supporting information (Section S3).

Attending to the PVOH incorporation method, the challenge of reducing the solid skin has been accomplished regardless of the technique used, providing the thermoforming slightly better results. Probably, the higher efficiency of that method is related to an appropriate adhesion between PMMA and PVOH as it has been demonstrated by in-situ visualization as well as SEM micrographs (see Supporting Information, Section S2). In addition to provide the best results, it should be noticed that the thermoforming method is a straightforward methodology in order to scale the PVOH technique for industrial gas dissolution foaming processes.

As a consequence of the solid skin reduction, several features of the PMMA foams obtained with PVOH coating were enhanced. For instance, the increase of the foamed region and the higher gas concentration available at the foaming stage allow obtaining larger expansions and therefore higher density reductions. Fig. 4 shows the direct relationship between the relative density and the non-foamed region. As expected, increasing the foamed region, i.e., reducing the appearance of the non-foamed solid skin, decreases the relative density of the whole sample. In fact, a direct correlation between both relative density and NFR was found (Fig. 4). Moreover, although the samples present an apparent solid skin of several microns, it has been proved that the incorporation of the PVOH barrier induces porous surfaces in PMMA (i.e., the remaining apparent solid skin is also partially foamed). Fig. 5 shows the comparison between the PMMA external surfaces of samples foamed using or not the PVOH approach. A smooth surface was obtained by foaming the PMMA according to the classic methodology (Fig. 5a), while a porous surface with an average cell size of around 2 µm was achieved by incorporating the PVOH gas barrier on that surface (Fig. 5b). The explanation of this substantial difference could be linked to the combination of two phenomena. First, the CO_2 concentration on the PMMA near the interface is high enough for the generation of cells by homogenous nucleation. Second, the interface between both PMMA and PVOH during the nucleation process could be inducing the heterogeneous nucleation of cells on the PMMA surface [56]. In this case, the energy barrier to generating cells could be sharply reduced in the interface allowing the foaming in the PMMA surface [1,57].

Table 2
Comparative of the analysis of the five regions along the thickness in the sampled showed in Fig. 3.

Region	Cell density 2D (cells/cm^2)	Cell density 3D (cells/cm^3)	Cell size (µm)	SD	Porosity
1 (top)	7.73×10^5	6.80×10^8	0.734	0.249	0.003
2 (top-middle)	3.30×10^6	5.99×10^9	2.169	1.002	0.122
3 (middle)	6.08×10^6	1.50×10^{10}	2.300	0.995	0.253
4 (bottom-middle)	5.36×10^6	1.24×10^{10}	3.217	1.394	0.436
5 (bottom)	4.64×10^6	9.99×10^9	3.636	1.201	0.482

Table 3
List of samples used to test the PVOH as gas diffusion barrier in PMMA, indicating the coating method, the original thickness of PMMA, the gas barrier thickness, the average non-foamed skin thickness, and the percentage of NFR of PMMA.

Sample	PVOH coating technique	Original PMMA thickness (μm)	PVOH thickness of each side (μm)	Average of non-foamed skin thickness (μm)	NFR (%)
PMMA + PVOH coating	Solvent casting	430	200	14.1 ± 2.6	2.6 ± 0.5
PMMA + PVOH coating	Thermoforming	545	200	11.3 ± 5.4	2.6 ± 1.3
PMMA	–	453	–	77.5 ± 7.4	21.2 ± 2.0

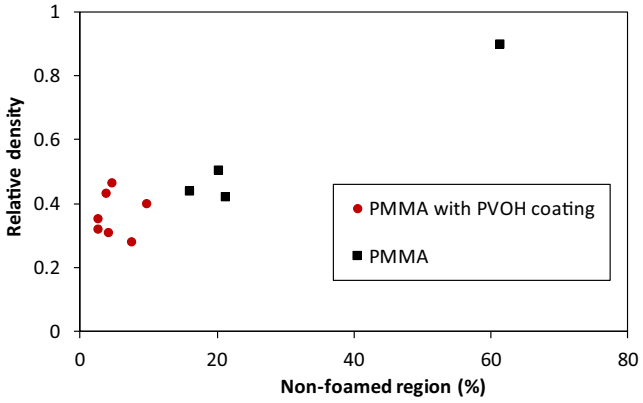

Fig. 4. Relationship between relative density and NFR by adding PVOH technique in PMMA foams.

Therefore, the addition of PVOH on the surface of PMMA as a gas diffusion barrier was demonstrated to be an effective approach to reduce the relative density by decreasing the non-foamed skin and creating cells on the surface. Indeed, it can be considered that the solid skin is partially foamed attending to the cell size of the surface porosity with an average cell size around 2 μm (Fig. 5b).

3.3. Foaming of thin films

Foaming of thin polymer films by gas dissolution foaming is one of the objectives of the present work. However, the fast gas diffusivity in the desorption stage generally hindered the foaming in very thin samples. This situation is exemplified in Fig. 6a, where just a few pores appeared in the center of the film, leaving a large volume without any cellular structure in both top and bottom halves. On the other hand, a PMMA film almost completely foamed with homogenous cellular structure was achieved by introducing the PVOH coating technique on both sides with the highest surface area (Fig. 6b). In particular, films fabricated by PVOH technique present nucleation densities in the order of 10^{13} nuclei/cm^3 and cell sizes in the nanometric range, similar to bulk samples at the same conditions and very close to precedent works which use optimized foaming parameters [9].

As it can be seen in Table 4, the average non-foamed skin has been reduced more than fourfold in PMMA thin films from 27 to 6 μm, inasmuch as the gas concentration prior to foaming in PMMA was raised in the whole film as a consequence of the gas diffusion limitation. Besides, both NFR and relative density were decreased from 61% to 7% and from 0.9 to 0.3, respectively, by introducing a PVOH coating of 50 μm (Table 4). Also, a smooth solid surface was showed by the PMMA film foamed using the traditional method without PVOH (Fig. 7a), while porous surfaces were obtained in the external surfaces in which PVOH was placed (Fig. 7b).

Therefore, the use of PVOH as a gas diffusion barrier proved to be a successful approach to overcome the limitations related to the foaming of thin films by gas dissolution foaming. Also, large expansions were reached in cellular polymers films by using a flexible diffusion barrier instead of the stiff barriers used in the past [58], which clearly hinder obtaining low-density cellular polymers.

Accordingly, the achieved reduction of the non-foamed skins in films and bulk cellular polymers fabricated by gas dissolution foaming is a remarkable step forward for the production of these materials, which could be even further exploited by the optimization of the foaming parameters. In addition, another significant advantage related to the PVOH incorporation over the PMMA surfaces has been provided by this work. The obtained results have confirmed the possibility of inducing the formation of cells directly on the external surfaces, both in films and bulk samples, which could interconnect the inner cellular structure with the external medium. For instance, reaching that feature with high-porosity nanofoams [16,59] could result in materials with excellent features for applications such as membranes, filters, or sensors. Finally, it can be highlighted that the results obtained with this approach

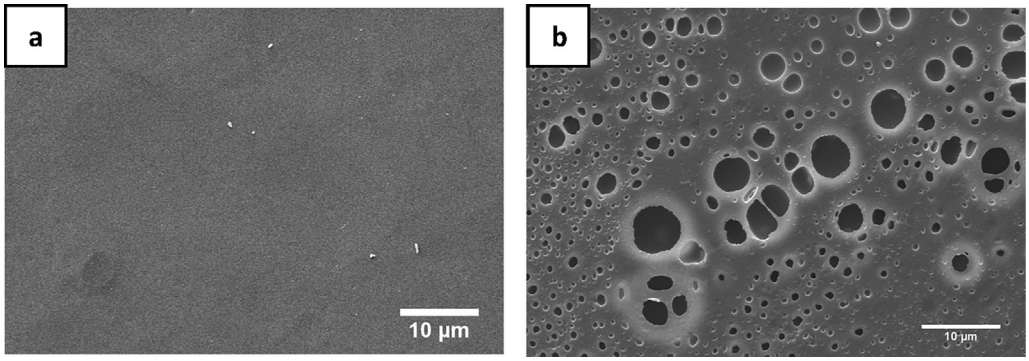

Fig. 5. SEM micrographs of PMMA foam external surface a) without using PVOH and b) using PVOH as a gas diffusion barrier.

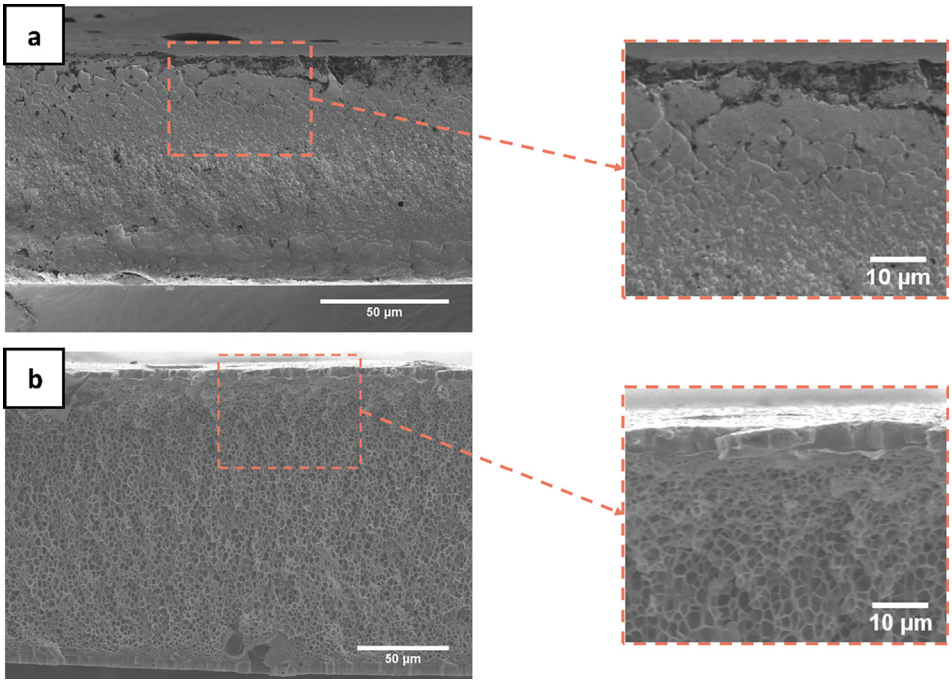

Fig. 6. Comparative of SEM micrographs between **a)** a PMMA film scarcely foamed without using the PVOH coating as a gas diffusion barrier and **b)** a PMMA film completely foamed using the PVOH coating as a gas diffusion barrier.

Table 4
Comparative of solid skin thickness, non-foamed region, and relative density between PMMA thin film, showing the original thickness of PMMA and PVOH.

Sample	PMMA original thickness (µm)	PVOH thickness (µm)	Average of non-foamed skin thickness (µm)	NFR (%)	Relative density
PMMA film	76	–	27.1 ± 2.7	61.4 ± 6.1	0.899
PMMA film with PVOH coating	46	50	6.3 ± 0.3	7.6 ± 0.3	0.280

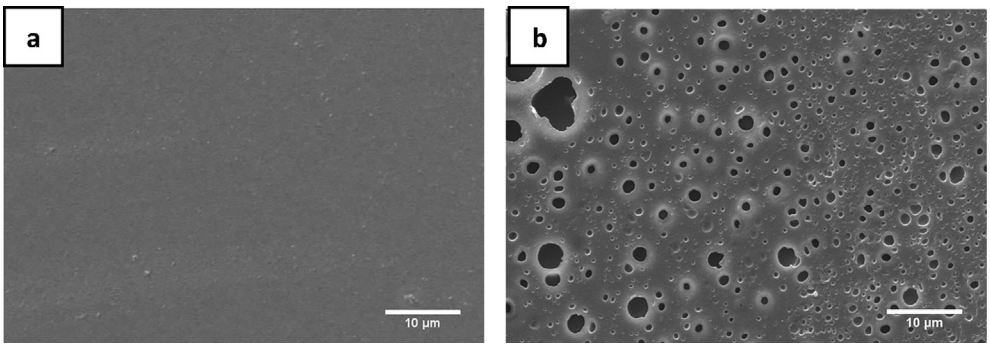

Fig. 7. SEM micrographs of PMMA foamed films surfaces **a)** without using PVOH and **b)** using PVOH as a gas diffusion barrier.

were successfully generalized using diverse polymer matrices, such as PC, PS, and PCL (see Supporting Information, Section S4).

4. Conclusions

The classical process of the gas dissolution foaming was successfully modified by designing a foaming procedure that introduces a flexible gas diffusion barrier in the borders of the polymer. This barrier is capable of reducing the gas diffusivity during the desorption step and avoiding the appearance of the non-foamed solid skins.

In this way, the typical non-foamed solid skins of bulk samples formed in the conventional foaming procedures were decreased from several tens to a few microns regardless the PVOH incorporation method, achieving by the thermoforming approach the best results. On the other hand, homogenous and completely foamed thin films were obtained by using the designed approach, which currently is the only successful approach to produce such samples.

Besides, the gas diffusion barrier induced a heterogeneous nucleation in the polymer surfaces, creating cells in the order magnitude of the reduced solid skins. Therefore, this feature would allow interconnecting the inner cellular structure with the external medium, extending the range of applications of cellular polymers produced by gas dissolution foaming, which are currently limited, due to the outer solid skins, for applications such as filtration, gas storage, or catalysis.

Declaration of Competing Interest

The authors declare that they have no known competing financial interests or personal relationships that could have appeared to influence the work reported in this paper.

Acknowledgements

This work was supported by the Regional Government of Castilla y León and the EU-FEDER program (CLU-2019-04).

Financial assistance from Ministerio de Ciencia e Innovación (Spain) (PRE2019-088820), Ministerio de Ciencia, Innovación y Universidades (MCIU) (Spain), FEDER (EU) (RTI2018 - 098749-B-I00 and RTI2018 - 097367-A-I00), and Ente Regional de la Energía de Castilla y León (EREN) (Spain) (EREN_2019_L4_UVA) are gratefully acknowledged.

Appendix A. Supplementary material

Supplementary data to this article can be found online at https://doi.org/10.1016/j.matdes.2022.110648.

References

[1] S. Costeux, CO2-blown nanocellular foams, J. Appl. Polym. Sci. 131 (23) (2014) n/a–n/a.
[2] J. Martín-de León, V. Bernardo, M. Rodríguez-Pérez, Nanocellular Polymers: The Challenge of Creating Cells in the Nanoscale, Materials (Basel) 12 (2019) 797, https://doi.org/10.3390/ma12050797.
[3] V. Kumar, N.P. Suh, A process for making microcellular thermoplastic parts, Polym. Eng. Sci. 30 (1990) 1323–1329, https://doi.org/10.1002/pen.760302010.
[4] D. Eaves, Handbook of polymer foams, Rapra Technology Limited (1993), https://doi.org/10.1002/pola.1993.080310535.
[5] K.A. Arora, A.J. Lesser, T.J. McCarthy, Preparation and Characterization of Microcellular Polystyrene Foams Processed in Supercritical Carbon Dioxide, Macromolecules 31 (14) (1998) 4614–4620.
[6] J.E. Weller, V. Kumar, Solid-state microcellular polycarbonate foams. I. The steady-state process space using subcritical carbon dioxide, Polym. Eng. Sci. 50 (2010) 2160–2169, https://doi.org/10.1002/pen.21736.
[7] H. Guo, A. Nicolae, V. Kumar, Solid-state microcellular and nanocellular polysulfone foams, J. Polym. Sci. Part B Polym. Phys. 53 (2015) 975–985, https://doi.org/10.1002/polb.23719.
[8] S.K. Yeh, Y.R. Chen, T.W. Kang, T.J. Tseng, S.P. Peng, C.C. Chu, S.P. Rwei, W.J. Guo, Different approaches for creating nanocellular TPU foams by supercritical CO2 foaming, J. Polym. Res. 25 (2018) 1–12, https://doi.org/10.1007/s10965-017-1419-9.
[9] J. Martín-de León, V. Bernardo, M. Rodríguez-Pérez, Low Density Nanocellular Polymers Based on PMMA Produced by Gas Dissolution Foaming Fabrication and Cellular Structure Characterization, Polymers (Basel) 8 (2016) 265, https://doi.org/10.3390/polym8070265.
[10] R.A. D. Klempner, Vahid Sendijarevi'c, Handbook of polymeric foams and foam technology, Choice Rev. Online. 42 (2004) 42-1564-42–1564. https://doi.org/10.5860/choice.42-1564.
[11] S. Deshmukh, H. Ronge, S. Ramamoorthy, Design of periodic foam structures for acoustic applications: Concept, parametric study and experimental validation, Mater. Des. 175 (2019), https://doi.org/10.1016/j.matdes.2019.107830 107830.
[12] S.-K. Yeh, Y.-C. Liu, C.-C. Chu, K.-C. Chang, S.-F. Wang, Mechanical Properties of Microcellular and Nanocellular Thermoplastic Polyurethane Nanocomposite Foams Created Using Supercritical Carbon Dioxide, Industrial & Engineering Chemistry Research 56 (30) (2017) 8499–8507.
[13] B. Notario, J. Pinto, M.A. Rodriguez-Perez, Nanoporous polymeric materials: A new class of materials with enhanced properties, Prog. Mater. Sci. 78–79 (2016) 93–139, https://doi.org/10.1016/j.pmatsci.2016.02.002.
[14] F.A. Almeida, H. Beyrichen, N. Dodamani, R. Caps, A. Müller, R. Oberhoffer, Thermal conductivity analysis of a new sub-micron sized polystyrene foam, J. Cell. Plast. 57 (4) (2021) 493–515.
[15] L.J.M. Jacobs, M.F. Kemmere, J.T.F. Keurentjes, Sustainable polymer foaming using high pressure carbon dioxide: A review on fundamentals, processes and applications, Green Chem. 10 (2008) 731–773, https://doi.org/10.1039/b801895b.
[16] D. Cuadra-Rodriguez, S. Barroso-Solares, J. Pinto, Advanced Nanocellular Foams: Perspectives on the Current Knowledge and Challenges, Nanomaterials. 11 (2021) 621, https://doi.org/10.3390/nano11030621.
[17] V. Kumar, J.E. Weller, A model for the unfoamed skin on microcellular foams, Polym. Eng. Sci. 34 (1994) 169–173, https://doi.org/10.1002/pen.760340302.
[18] J. Pinto, M. Dumon, M.A. Rodriguez-Perez, R. Garcia, C. Dietz, Block copolymers self-assembly allows obtaining tunable micro or nanoporous membranes or depth filters based on PMMA; Fabrication method and nanostructures, J. Phys. Chem. C. 118 (2014) 4656–4663, https://doi.org/10.1021/jp409803u.
[19] J. Pinto, D. Morselli, V. Bernardo, B. Notario, D. Fragouli, M.A. Rodriguez-Perez, A. Athanassiou, Nanoporous PMMA foams with templated pore size obtained by localized in situ synthesis of nanoparticles and CO2 foaming, Polymer (Guildf). 124 (2017) 176–185, https://doi.org/10.1016/J.POLYMER.2017.07.067.
[20] J. Germain, J.M.J. Fréchet, F. Svec, Nanoporous Polymers for Hydrogen Storage, Small. 5 (2009) 1098–1111, https://doi.org/10.1002/smll.200801762.
[21] G.Q. Lu, Chapter 1 NANOPOROUS MATERIALS - AN OVERVIEW, Nanoporous Mater. Proc. 5th Int. Symp. Vancouver, Canada, 25-28 May 2008. (2008).
[22] B. Notario, A. Ballesteros, J. Pinto, M.A. Rodríguez-Pérez, Nanoporous PMMA: A novel system with different acoustic properties, Mater. Lett. 168 (2016) 76–79, https://doi.org/10.1016/J.MATLET.2016.01.037.
[23] C.P. Park, Cellular acoustic absorption polymer foam having improved thermal insulating performance, 2001. https://patents.google.com/patent/US20010036970?oq=skin+reduction+in+cellular+polymers (accessed August 28, 2019).
[24] P. Huang, F. Wu, B. Shen, X. Ma, Y. Zhao, M. Wu, J. Wang, Z. Liu, H. Luo, W. Zheng, Bio-inspired lightweight polypropylene foams with tunable hierarchical tubular porous structure and its application for oil-water separation, Chem. Eng. J. 370 (2019) 1322–1330, https://doi.org/10.1016/J.CEJ.2019.03.289.
[25] F. Wu, P. Huang, H. Luo, J. Wang, B. Shen, Q. Ren, P. He, H. Zheng, L. Zhang, W. Zheng, Novel lightweight open-cell polypropylene foams for filtering hazardous materials, RSC Adv. 10 (2020) 17694–17701, https://doi.org/10.1039/d0ra01499k.
[26] C.P. Park, Perforated foams, 1999. https://patents.google.com/patent/US6720362B1/en?q=Perforated&q=plastic&q=foam&q=manufacturing&q=process&patents=false&oq=Perforated+plastic+and+foam+manufacturing+process (accessed August 28, 2019).
[27] R. Zhang, J. Chen, Y. Zhu, J. Zhang, G. Luo, P. Cao, Q. Shen, Correlation Between the Structure and Compressive Property of PMMA Microcellular Foams Fabricated by Supercritical CO 2 Foaming Method, (2020) 1–14. https://doi.org/10.3390/polym12020315.
[28] J. Martín-de León, V. Bernardo, M.Á. Rodríguez-Pérez, Key Production Parameters to Obtain Transparent Nanocellular PMMA, Macromol. Mater. Eng. 302 (2017) 3–7, https://doi.org/10.1002/mame.201700343.
[29] S.K. Yeh, Z.E. Liao, K.C. Wang, Y.T. Ho, V. Kurniawan, P.C. Tseng, T.W. Tseng, Effect of molecular weight to the structure of nanocellular foams: Phase separation approach, Polymer (Guildf). 191 (2020), https://doi.org/10.1016/j.polymer.2020.122275 122275.
[30] A. Nicolae, H.M. Guo, V. Kumar, Method of calculating the fluid permeability of machined skin-covered porous sheets from experimental flow data, Int. Polym. Process. 32 (2017) 355–362, https://doi.org/10.3139/217.3352.
[31] P.A. Kolosowski, Method for providing accelerated release of a blowing agent from a plastic foam, 1995. https://patents.google.com/patent/US5585058 (accessed August 29, 2019).
[32] S.-T. Lee, M. Brandolini, Partially perforated foam, (1999). https://patents.google.com/patent/US6207254B1/en?oq=skin+reduction+in+cellular+polymers (accessed August 29, 2019).
[33] H. Yokoyama, T.E. Mates, E.J. Kramer, Structure of Asymmetric Diblock Copolymers in Thin Films, (2000). https://doi.org/10.1021/ma9912047.
[34] D. Jose, C. Gutierrez, FABRICATION OF BULK SKINLESS POLYETHERIMIDE (PEI) NANOFOAMS, in: Proceedings of the ASME 2016 International Mechanical Engineering Congress and Exposition IMECE2016, 2017: pp. 1–8. https://doi.org/doi.org/10.1115/IMECE2016-66055.
[35] S. Orsi, E. Di Maio, S. Iannace, P.A. Netti, Hollow micro- and nano-particles by gas foaming, Nano Res. 7 (2014) 1018–1026, https://doi.org/10.1007/s12274-014-0465-4.
[36] J. Yang, T. Jiang, B. Liu, C. Zhang, X. Zeng, L. He, W. Gong, Experimental and numerical analysis of bubble nucleation in foaming polymer, Mater. Des. 203 (2021), https://doi.org/10.1016/j.matdes.2021.109577 109577.
[37] S. Siripurapu, J.A. Coughlan, R.J. Spontak, S.A. Khan, Surface-constrained foaming of polymer thin films with supercritical carbon dioxide, Macromolecules. 37 (2004) 9872–9879, https://doi.org/10.1021/ma0484983.
[38] M. Morisaki, T. Ito, M. Hayvali, I. Tabata, K. Hisada, T. Hori, Preparation of skinless polymer foam with supercritical carbon dioxide and its application to a photoinduced hydrogen evolution system, Polymer (Guildf). 49 (2008) 1611–1619, https://doi.org/10.1016/J.POLYMER.2008.01.049.
[39] C. Ge, W. Zhai, C.B. Park, Preparation of Thermoplastic Polyurethane (TPU) Perforated Membrane via CO2 Foaming and Its Particle Separation Performance, Polymers (Basel). 11 (2019) 847, https://doi.org/10.3390/polym11050847.
[40] W.-H. Lin, T.-S. Chung, Gas permeability, diffusivity, solubility, and aging characteristics of 6FDA-durene polyimide membranes, J. Memb. Sci. 186 (2001) 183–193, https://doi.org/10.1016/S0376-7388(01)00333-7.
[41] Y. Liu, R. Wang, T.-S. Chung, Chemical cross-linking modification of polyimide membranes for gas separation, J. Memb. Sci. 189 (2001) 231–239, https://doi.org/10.1016/S0376-7388(01)00415-X.
[42] S. Barroso-Solares, D. Cuadra-Rodriguez, M.L. Rodriguez-Mendez, M.A. Rodriguez-Perez, J. Pinto, A new generation of hollow polymeric microfibers

produced by gas dissolution foaming, J. Mater. Chem. B. 8 (2020) 8820–8829, https://doi.org/10.1039/d0tb01560a.
[43] Y.-G. Zhou, T.-Y. Chen, M. Mechanical Equipment, C. Ying-Guo Zhou, Combining foam injection molding with batch foaming to improve cell density and control cellular orientation via multiple gas dissolution and desorption processes, Polym. Adv. Technol. 31 (2020) 2136–2151, https://doi.org/10.1002/PAT.4935.
[44] J. Martín-de León, V. Bernardo, M.Á. Rodriguez-Perez, Cyclic gas dissolution foaming as an approach for simultaneously reducing cell size and relative density in nanocellular pmma, Polymers (Basel) 13 (14) (2021) 2383.
[45] D. Cuadra-Rodríguez, D. Carrascal, E. Solórzano, M.A.R. Pérez, J. Pinto, Analysis of the retrograde behavior in PMMA-CO2 systems by measuring the (effective) glass transition temperature using refractive index variations, J. Supercrit. Fluids. 170 (2021), https://doi.org/10.1016/j.supflu.2020.105159 105159.
[46] S. Cotugno, E. Di Maio, G. Mensitieri, S. Iannace, G.W. Roberts, R.G. Carbonell, H.B. Hopfenberg, Characterization of microcellular biodegradable polymeric foams produced from supercritical carbon dioxide solutions, Ind. Eng. Chem. Res. 44 (2005) 1795–1803, https://doi.org/10.1021/ie049445c.
[47] G. Li, J. Wang, C.B. Park, R. Simha, Measurement of gas solubility in linear/branched PP melts, J. Polym. Sci. Part B Polym. Phys. 45 (2007) 2497–2508, https://doi.org/10.1002/polb.21229.
[48] D. Kohlhoff, A. Nabil, M. Ohshima, In situ preparation of cross-linked polystyrene/poly(methyl methacrylate) blend foams with a bimodal cellular structure, Polym. Adv. Technol. 23 (2012) 1350–1356, https://doi.org/10.1002/pat.2053.
[49] H. Guo, A. Nicolae, V. Kumar, Solid-state poly(methyl methacrylate) (PMMA) nanofoams. Part II: Low-temperature solid-state process space using CO2 and the resulting morphologies, Polymer (Guildf). 70 (2015) 231–241, https://doi.org/10.1016/J.POLYMER.2015.06.031.
[50] J.A. Reglero Ruiz, M. Dumon, J. Pinto, M.A. Rodriguez-Pérez, Low-density nanocellular foams produced by high-pressure carbon dioxide, Macromol. Mater. Eng. 296 (8) (2011) 752–759.
[51] M.D. Abràmoff, P.J. Magalhães, S.J. Ram, Image processing with imageJ, Biophotonics Int. 11 (2004) 36–41, https://doi.org/10.1201/9781420005615.ax4.
[52] J. Pinto, E. Solórzano, M.A. Rodriguez-Perez, J.A. de Saja, Characterization of the cellular structure based on user-interactive image analysis procedures, J. Cell. Plast. 49 (6) (2013) 555–575.
[53] V. Kumar, N.P. Suh, Process Synthesis for Manufacturing Microcellular Thermoplastic Parts: a Case Study in Axiomatic Design., (1988).
[54] C.A. Mandarim-de-Lacerda, Stereological tools in biomedical research, An. Acad. Bras. Cienc. 75 (2003) 469–486, https://doi.org/10.1590/S0001-37652003000400006.
[55] G. Das, Image analysis in quantitative metallography, Mater. Charact. Tech. Appl. 831007 (1999) 135–150.
[56] C. Ge, W. Zhai, C.B. Park, Preparation of Thermoplastic Polyurethane (TPU) Perforated Membrane via CO2 Foaming and Its Particle Separation Performance, (2019).
[57] J.S. Colton, N.P. Suh, The nucleation of microcellular thermoplastic foam with additives: Part I: Theoretical considerations, Polym. Eng. Sci. 27 (1987) 485–492, https://doi.org/10.1002/pen.760270702.
[58] S. Siripurapu, J.M. DeSimone, S.A. Khan, R.J. Spontak, Controlled foaming of polymer films through restricted surface diffusion and the addition of nanosilica particles or CO 2-philic surfactants, Macromolecules. 38 (2005) 2271–2280, https://doi.org/10.1021/ma047991b.
[59] Z. Shi, X. Ma, G. Zhao, G. Wang, L. Zhang, B. Li, Fabrication of high porosity Nanocellular polymer foams based on PMMA/PVDF blends, Mater. Des. 195 (2020), https://doi.org/10.1016/j.matdes.2020.109002 109002.